Synthesis and Study the Structural and Magnetic Properties of Cobalt Substituted Strontium Hexaferrite

Ali M. Mohammad*

University of Garmian, College of Education, Department of Physics, Kurdistan region, Iraq.

ABSTRACT

A sol-gel auto combustion approach was used to synthesize Co^{2+} substituted M-type strontium hexagonal ferrite with the chemical formula $Sr_{1-x}Co_xFe_{12}O_{19}$ (x=0.0, 0.25, 0.50 and 0.75). X-ray Diffraction (XRD), Field Emission Scanning Electron Microscopy (FE-SEM), Raman Spectroscopy and Vibrating Sample Magnetometer (VSM) have been used to investigate the structural and magnetic properties as a function of cobalt ions substitution in Sr-hexaferrite. XRD pattern disclosed a single M-type hexagonal crystalline phase at x=0, while a desired phase of the strontium M-type hexaferrite with undesired phase appeared with the increase of the cobalt contents. FE-SEM images showed that the particles have irregular distribution and non-uniform shape. Generally, the cobalt ions substitution does not alter the surface morphology. The Raman spectra measurement proved the formation of magnetoplumbite structure of $Sr_{1-x}Co_xFe_{12}O_{19}$ system. The pure strontium hexaferrite compound showed sharp and intense peaks. The intensity of the peaks decreased when the Co^{2+} ions contents increased. VSM measurements showed ferromagnetic properties for all synthesized samples. The magnetic properties such as saturation magnetization (M_S), remanence magnetization (M_r), coercive field (H_c), effective anisotropy constant (K_{eff}), anisotropy field (H_a), and squareness ratio (S) showed a progressive decrease with the increase of the cobalt ions substitution in the M-type strontium hexaferrite system. Replacement of strontium (Sr) by cobalt (Co) ions weakens the super-exchange interactions among particles.

Keywords: Sol-Gel Auto Combustion Method, Strontium Hexaferrite, Raman Spectra Measurement, Magnetic Properties

1. INTRODUCTION

Ferrites are now extremely important and powerful materials owing to their unique magnetic and electrical properties. These features make them very suitable for technological applications. In recent years, the hexagonal crystal structure has been paid much more attention and increased exponentially due to their excellent properties. The M-type hexaferrite is treated as a class of hard magnetic materials and participated reliably in distinct hi-tech and manufacturing fields due to their chemical strength, high uniaxial magneto-crystalline anisotropy and low cost with simple production routes [1]. $SrFe_{12}O_{19}$ hexaferrite has high magnetocrystalline anisotropy, large coercive force value, remanence, and Curie temperature. These properties widen their usage for various applications such as magneto-optic devices, magnetic recording media, transformer cores, and microwave absorbing [2]. The hard magnetic property of the M-type hexaferrite is attributed to the uniaxial magneto-crystalline anisotropy of Fe^{3+} ions [3] distributed through five symmetry sites: three octahedral (↑12k, ↑2a and ↓4f2), one tetrahedral

*E-mail: ali.mustafa@garmian.edu.krd

($\downarrow$4f1), and one trigonal bipyramidal ($\uparrow$2b) [4]. The substitution of the element and synthesis method were found to influence the magnetic property of hexaferrite [5]. For better magnetic properties, abundant attempts have been made such as the substitution of divalent-tetravalent and trivalent cationic to replace the Fe^{3+} ions distributed at the five different crystallographic sub-lattices [6]. Generally, various methods have been used to prepare ferrites materials such as co-precipitation [7], micro-emulsion routes [8], hydrothermal [9] and sol-gel combustion method [10]. These methods play an important role in the structure, magnetic and morphology properties. In this study, the focus is on the synthesis of M-type hexaferrite $Sr_{1-x}Co_xFe_{12}O_{19}$ (x=0.0, 0.25, 0.50 and 0.75) carried out by sol-gel auto combustion method. The effects of cobalt ions substitution on structural and magnetic properties have been studied.

2. EXPERIMENTAL PROCEDURE

$Sr_{1-x}Co_xFe_{12}O_{19}$ hexaferrite (x=0.0, 0.25, 0.50 and 0.75) was synthesized using citrate sol-gel auto combustion method. A stoichiometric amount of Sr, Co and Fe nitrates were dissolved at a minimum amount of deionized water under constant stirring. Citric acid solution ($C_6H_8O_7$) was added to the mixed solution as fuel. The pH of the final solution was adjusted to 7 using ammonia solution and heated to 90°C to let all water evaporate and leave a viscous dense gel. The final viscous gel was heated to 275°C so that auto-combustion occurs and forms a fluffy powder. Ultimately, the resulting powder was calcined at 900°C for 4 hours to form $Sr_{1-x}Co_xFe_{12}O_{19}$ hexaferrite phase. The identification of the crystalline phase was performed using X-ray Diffraction (XRD), model PANalytical (X'pert Pro, Netherlands) with Cu-kα radiation source, in the range of 20°–80°. Raman spectroscopy (Micro-Raman spectroscopy-785 nm laser) was used to investigate the vibrational spectra of all samples while the surface morphology was investigated using FE-SEM (FE-SEM; Model Mira3-XMU, TESCAN, Japan). Magnetic measurements were carried out at room temperature using vibrating sample magnetometer (VSM) (LBKFB model Meghnatis Daghigh Kavir Company).

3. RESULTS AND DISCUSSION

3.1 X-ray Diffraction (XRD)

XRD patterns of $Sr_{1-x}Co_xFe_{12}O_{19}$ hexaferrite (x=0.0, 0.25, 0.50 and 0.75) calcined at 900°C are shown in Figure 1. The given XRD pattern of pure Sr hexaferrite (x=0.0) reveals the diffraction peaks from the plains (006), (110), (107), (114), (201), (203), (205), (206), (217), (2011) and (220) which exhibits the characteristic peaks similar to the M-type of single hexagonal pure strontium ferrite structure (ICDD 01-079-1411). It is clear that the well-defined, sharp and intense peaks indicate a good crystalline. The XRD patterns of cobalt substituted strontium hexaferrite (x=0.25, 0.50 and 0.75) display a desired phase of the strontium M-type hexaferrite and an undesired phase as the second phase hematite (Fe_2O_3). It can be assumed that during the calcinations, magnetite oxidizes turn into very stable non-magnetic hematite [11]. In addition, it is clear that the peak intensities alternate by substitution of cobalt ions. The position of the peak gradually shifts towards lower position compared to the un-substituted sample possibly due to the substitution of Co with the Sr ions with different ionic radius. Also, this variation is mainly because of the crystallographic site's occupation in the crystal lattice. From Table 1, the value of lattice constant 'a' and 'b' remain the same for the hexaferrite system (x=0.0, 0.25, 0.50 and 0.75). The "c/a" relation range from 3.862 to 3.93, indicating that the unit cell volume becomes smaller as the Co^{+2} ions content increases. This behaviour may be assigned to the shrinkage of the $SrFe_{12}O_{19}$ crystalline lattice due to the large variation in ionic radii of the Sr compared to the Co ions.
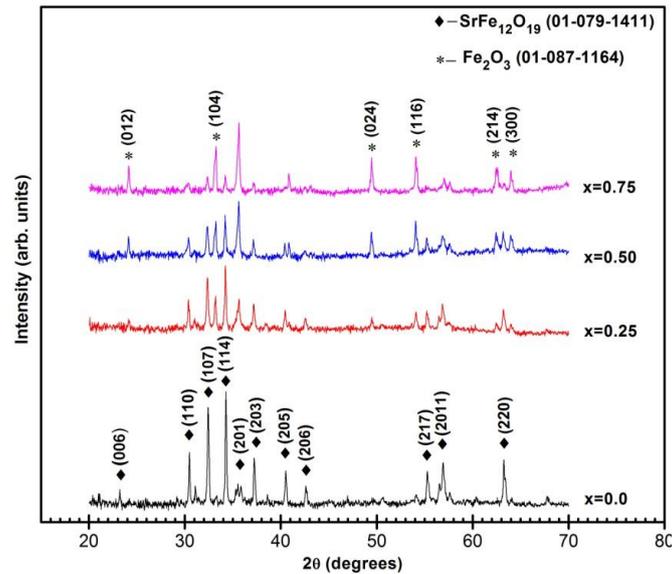
Figure 1. XRD pattern of $Sr_{1-x}Co_xFe_{12}O_{19}$ hexaferrite (x=0.0, 0.25, 0.50 and 0.75) at room-temperature.

Various parameters, i.e. the lattice parameters (*a*, *c* and *c/a)*, the crystallite size (*D*), unit cell volume (V_{cell}) and X-ray density (ρ_x), of all powder samples are estimated from the following formulae [12, 13].

$$\frac{1}{d^2} = \frac{4(h^2 + hk + k^2)}{3a^2} + \frac{l^2}{c^2} \tag{1}$$

$$D = \frac{0.9\,\lambda}{\beta \cos\theta} \tag{2}$$

$$V_{cell} = 0.8666\,a^2 \tag{3}$$

$$\rho_x = \frac{2\,M}{N_A\,V_{cell}} \tag{4}$$

where *a* and *c* are lattice constants, λ is the x-ray wavelength, β is the FWHM intensity, θ being diffraction angle in degree, *M* the molecular mass and N_A Avogadro's number.

Table 1 shows the variation of the average crystallite size as a function of Co^{2+} ions content ranged from 61.556- 49.058 nm. The observed crystallite size confirmed that the synthesis compound has nanocrystalline nature, the change in peaks' intensities indicate the compound variation**.**

Table 1. Structural parameters for $Sr_{1-x}Co_xFe_{12}O_{19}$ hexaferrite (x=0.0, 0.25, 0.50 and 0.75).

x	*a* (Å)	*c* (Å)	*c /a*	*D* (nm)	V_{cell} (Å³)	ρ_x (gm/cm³)
0.00	5.86676	23.0591	3.93	61.556	687.3174862	5.130
0.25	5.88286	23.0241	3.914	59.347	690.0445649	5.075
0.50	5.88132	23.113	3.93	46.332	692.346923	5.024
0.75	5.9005	22.785	3.862	49.058	686.981711	5.028

3.2   Surface Morphology

The morphological analysis of $Sr_{1-x}Co_xFe_{12}O_{19}$ hexaferrite (x=0.0, 0.25, 0.50 and 0.75) is shown in Figure 2. It is obvious from the figures that the particles have a well-defined shape. The shape becomes a hexagonal piece with aggregates of a sphere, plate-like and polyhedral shape. The irregular distribution and non-uniform manner in particles size may be due to the effect of the synthesis method. The rapid growth in the formation of crystalline hexaferrite using sol-gel auto combustion technique has led to the variation of particles size distribution that related to the length of time. Sufficient high temperature is required to complete the preparation [14]. It can be seen that the substitution of cobalt ions does not alter the surface morphology, however, it only reveals the existence of some agglomeration area. The presence of some agglomerated particles together in FE-SEM images is attributed to the existence of magnetic interactions between the particles [15]. The considerable decreases in the porosity of all samples are ascribed to the gathering of large masses.
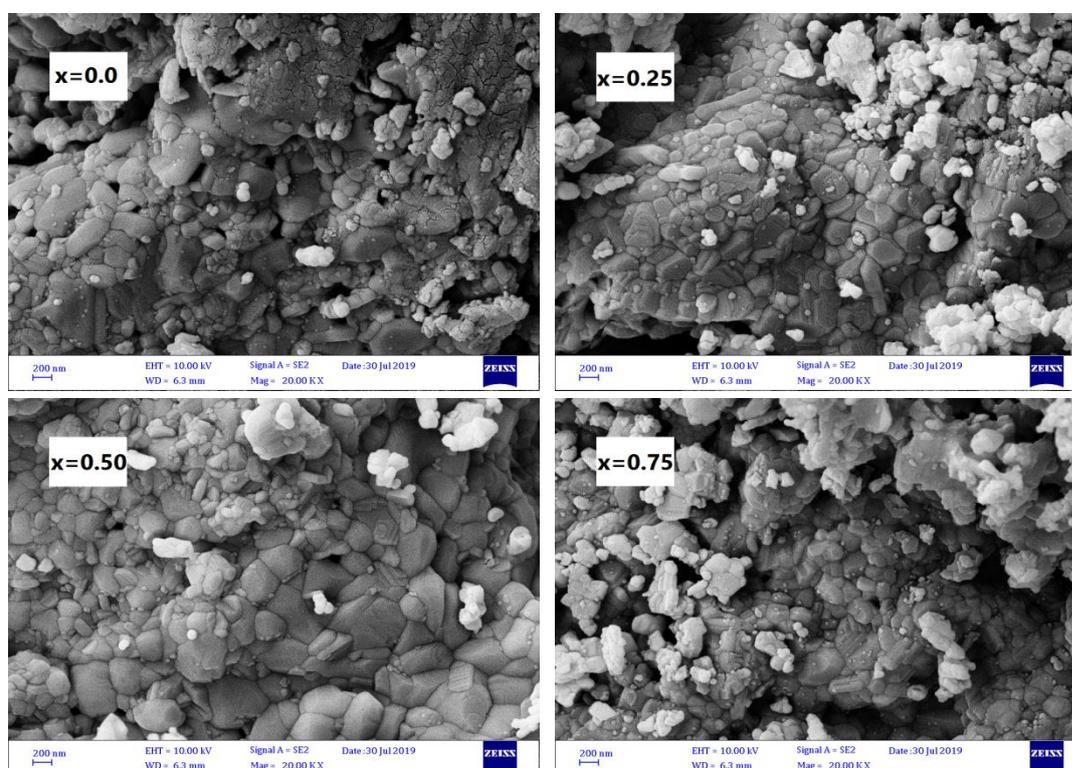

Figure 2. FE-SEM images of $Sr_{1-x}Co_xFe_{12}O_{19}$ hexaferrite (x=0.0, 0.25, 0.50 and 0.75).

An increase in the amount of substituted Co^{2+} ions may disrupt the structure of hexaferrite due to too much grain growth. This leads to the destruction of grain morphology and the change of particle size, thus the melting or/and adhesion phenomenon among particles can be accrued, and the material properties be influenced [16]. Due to the fact that the sizes of the crystals calculated according to the Scherrer equation are not very accurate, the FE-SEM images of the samples were recorded to be closer to reality.

3.3   Raman Measurements

Raman spectroscopy is an attractive method which involves a vibrational or rotational mode of the molecular and crystal lattice, therefore it is very sensitive to the composition, chemical environment, bonding, crystallite size, spin-lattice coupling, and charge-lattice. The unit cell of strontium hexaferrite (M-type) consists of 64 ions distributed on 11 different symmetry sites. It has 174 degrees of freedom, 3 of which correspond to the acoustic modes and the other 171

correlate to the optical modes. According to the literature, it is reported that there are 42 Raman-active modes ($11A_{1g}+14E_{1g}+17E_{2g}$), 30 IR active modes ($13A_{2u}+17E_{1u}$) and other modes are silent ($3A_{1u}+4A_{2g}+13B_{1g}+4B_{1u}+3B_{2g}+12B_{2u}+15E_{2u}$) [17]. Figure 3 shows the Raman spectra of all powder samples recorded at room temperature in the range of 150-1100 cm^{-1} for $Se_{1-x}Co_xFe_{12}O_{19}$ hexaferrite where x=0.0, 0.25, 0.50, and 0.75. The Raman vibration modes for pure $SrFe_{12}O_{19}$ hexaferrite exhibit sharp and more intense peaks compared to those substituted by Co ions, which reveal the defect-free environment. Their intensities decrease when the Co^{2+} ions substitution is increased and slightly shifted towards higher frequencies. The decrease in intensity with the increase of Co substitution probably related to the increase of lattice strain with an increase of Co in strontium hexaferrite [18]. Raman spectrum in Figure 3 for strontium hexaferrite (x=0.0) showed different vibration peaks at about 170, 202, 279, 327, 404, 460, 517, 606 and 677 cm^{-1}.
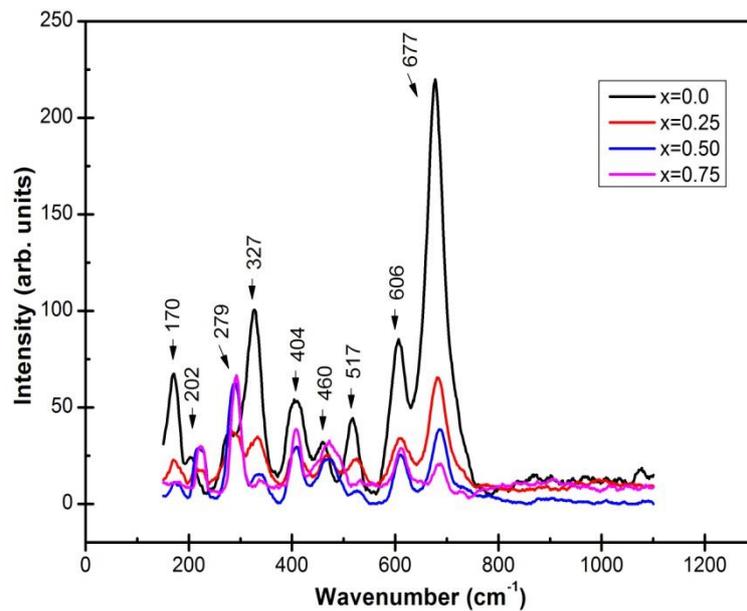
**Figure 3.** Raman spectra for $Sr_{1-x}Co_xFe_{12}O_{19}$ hexaferrite (x=0.0, 0.25, 0.50 and 0.75) at room temperature.

The peaks at 170 and 202 cm^{-1} are caused by E_{1g} vibration of the whole spinel block, while the peak at 279 cm^{-1} was due to E_{1g} vibration at the octahedral site. The peak at 327 cm^{-1} can be assigned to A_{1g} vibration at the octahedral 12k site. The peak at 404 cm^{-1} is owing to A_{1g} vibration at the octahedral 12k dominated site whereas the peaks at 460 and 517 cm^{-1} results from A_{1g} and E_{1g} vibrations of Fe-O bonds at the octahedral 2a sites respectively. The peak observed at 606 cm^{-1} refers to A_{1g} vibration mode related to the stretching vibration of Fe–O at the 4f2 octahedral sites. The intense vibration peak at 677 cm^{-1} assigned to A_{1g} vibrations of Fe-O bonds at bipyramidal 2b sites. Generally, Raman spectroscopy analysis confirmed that the pure Sr and its substituted compounds belong to the magnetoplumbite crystalline structure.

3.4   Magnetic Properties

Figure 4 shows the magnetic hysteresis loops of $Sr_{1-x}Co_xFe_{12}O_{19}$ (x=0.0, 0.25, 0.50 and 0.75) where the materials were measured under a magnetic field of ±15 KOe at room temperature. All of the studied samples exhibited familiar magnetic hysteresis behaviour. It is also worth noting that the room temperature magnetization of all substituted ferrite displays magnetic properties which are dependent on and highly related to Co^{2+} ions contents. The values of the saturation magnetization (M_s) for each sample was calculated from the magnetic hysteresis loops using the Stoner-Wohlfarth (S-W) model, which is applicable for a single domain [19, 20].
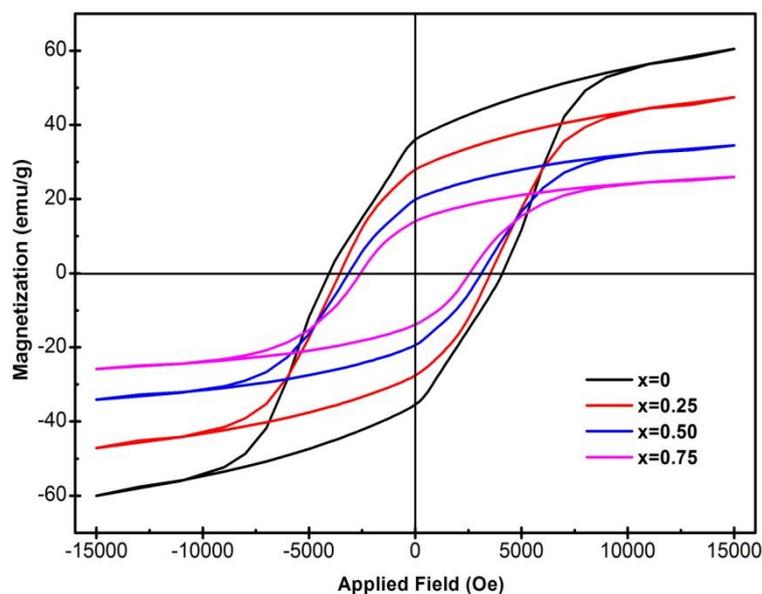
Figure 4. The applied-field dependence of the magnetization hysteresis loops of $Sr_{1-x}Co_xFe_{12}O_{19}$ hexaferrite (x=0.0, 0.25, 0.50 and 0.75) at room temperature.

Figure 5 represents a plot of M vs. $1/H^2$ for $Sr_{1-x}Co_xFe_{12}O_{19}$ hexaferrite (x=0.0, 0.25, 0.50 and 0.75). The value of M_s is estimated as the intercept of the linear fitting with M-axis at $1/H^2=0$. At an adequately high magnetic field, the magnetization (M), as a function of an applied magnetic field is presented as follows [14, 21]:

$$M = M_s \left[1 - \frac{B}{H^2}\right] \tag{5}$$

Then, consequently, the linear fitting in Eq. (5) supplies the slope (M_sB) (Figure 5) providing the constant B that is related to the magnetocrystalline anisotropy. From the slope, the values of B parameter is estimated and displayed in Table 2. Furthermore, determining the magnitudes of B parameter, the effective anisotropy constant (K_{eff}) for uniaxial magnetic hexagonal crystals can be calculated using Eq. (6) [22]:

$$K_{eff} = M_s \left(\frac{15\,B}{4}\right)^{1/2} \tag{6}$$

The anisotropy field (H_a) can be estimated from K_{eff} value using Eq. (7) [23]:

$$H_a = \frac{2\,K_{eff}}{M_s} \tag{7}$$

The variations of K_{eff} and H_a as a function of constants (x) are presented in Figure 6 (d) and 6 (e) respectively and listed in Table 2. The remanence magnetization (M_r), and coercivity (H_c) are determined from the obtained hysteresis loops respectively and tabulated in Table 2. Furthermore, the squareness ratio (S) was calculated using the following relation [24].

$$S = \frac{M_r}{M_s} \tag{8}$$

As shown in Table 2 and Figure 5, the highest value of saturation magnetization (M_s) is 63.49799 emu/g achieved at 15 KOe for un-substituted ($SrFe_{12}O_{19}$), while the lowest value is

26.99074 emu/g obtained in the same applied field for Co^{2+} substitutions at x=0.75. It was confirmed that the Co^{2+} ions substitutions significantly influence the saturation magnetization.
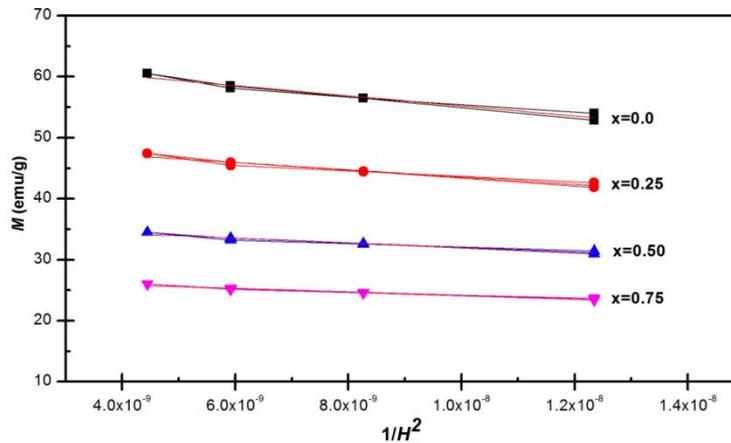

Figure 5. Magnetization (*M*) against $1/H^2$ plots for $Sr_{1-x}Co_xFe_{12}O_{19}$ hexaferrite (x=0.0, 0.25, 0.50 and 0.75).

The value of remanent magnetization (M_r) of all synthesized samples ranged from 36.0133 to 14.0366 emu/g (Table 2). The (M_r) values decline with the increase of Co^{2+} ions contents, which display a decrease with the increase of Co^{2+} ions contents. The values of coercive field (H_c) occurred in the range of 4051 to 2571 Oe from x=0.0 to x=0.75, respectively. From these results, one can conclude that the synthesized ferrite samples have ferromagnetic behaviour.

Table 2 Magnetic parameters of $Sr_{1-x}Co_xFe_{12}O_{19}$ hexaferrite (x=0.0, 0.25, 0.50 and 0.75)

X	M_s (emu/g)	M_r (emu/g)	H_c (Oe)	$B\times10^7$ (Oe^2)	$K\times10^3$ (emu .Oe g^{-1})	H_a (KOe)	M_r/M_s
0.00	63.49799	36.0133	4051	1.30	443.99	13.98	0.57
0.25	49.51833	27.9810	3543	1.20	332.73	13.44	0.57
0.50	35.82917	19.8673	3135	1.06	226.16	12.62	0.55
0.75	26.99074	14.0366	2571	1.05	169.73	12.58	0.52

The drop in M_s values (Figure 6 (a)) with the increase of cobalt ions contents is due to the replacement of Sr^{2+} by Co^{2+} ions and cations distributions. The discrepancies ionic radius of Co^{2+} (0.78 Å) and Sr^{2+} (1.18 Å) influence the ion-ion separations, therefore, the strength of the super-exchange interactions are weakened [25]. The observed reduction in M_r values (Figure 6 (b)) is primarily assigned to the alterations of M_s and overall arrangements of the grain magnetization are induced via grains and mediated weak exchange interactions [26]. In fact, the local strain can be produced by Co^{2+} ions substitution, producing the noncollinear ferromagnetic orientations or disturbing the magnetic spin moments at lattice sites [25]. As it is obvious in Figure 6 (c), the strengthening of uniaxial magneto-crystalline anisotropy along the c-axis is responsible for the high value of H_c for strontium hexaferrite sample (x=0). The sensitivity of c-axis is very high to the magnetic properties and anisotropy of Sr-hexaferrite [25, 26]. The values of H_c is highly affected by the variation of ions contents substitution as it decreased with the increase in the substitution ions levels. This observation was mostly attributed to the shrinkage of crystallites sizes, which was confirmed by the XRD analysis. Similar behaviours were also observed on other various ions substituted hexaferrite [16, 27].
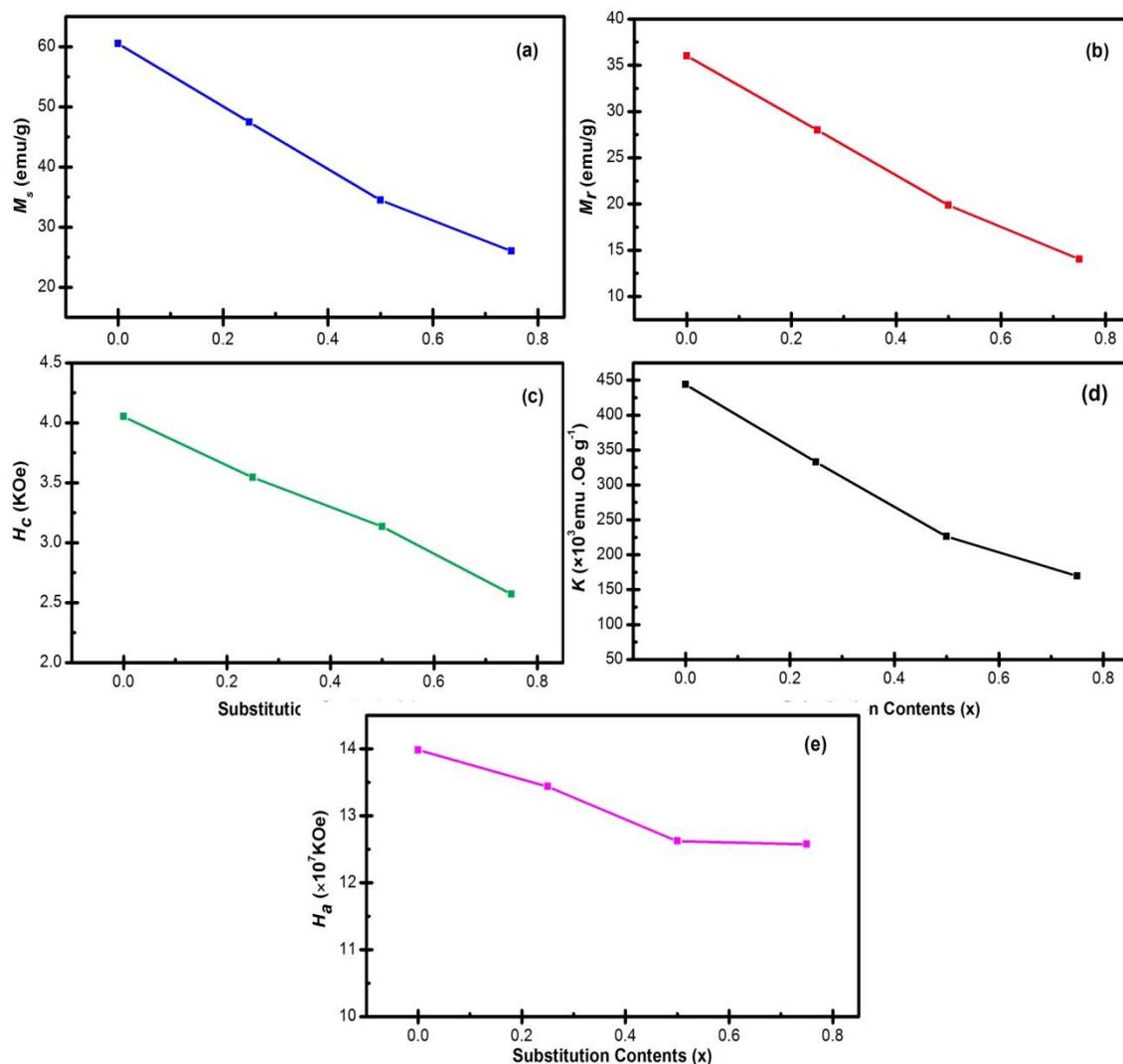
Figure 6. (a) Variation of saturation magnetization (M_s), (b) remanence (M_r), (c) coercive field (H_c), (d) effective anisotropy constant (K_{eff}) and (e) anisotropy field (H_a) as a function of substitution contents (x) for $Sr_{1-x}Co_xFe_{12}O_{19}$ hexaferrite.

In this study, the coercive field (H_c) is reduced as the concentration (x) elevates, all the more reasons to decrease the effective magnetic anisotropy. Previous studies showed that the substitutions of ions reduce the magneto-crystalline anisotropy through the decrease of the coercive field [5, 28]. Figure 4 (d) shows the variation of values of effective anisotropy constant (K_{eff}) which is dependent on the content of Co^{2+} ions in synthesis Sr-hexaferrite, wherein the value of K_{eff} was the largest for un-substituted $SrFe_{12}O_{19}$. Moreover, K_{eff} value reduced by increasing the Co^{2+} ions substitution, which was mainly associated with a decrease in the magnetic anisotropy sources which affects and weakens the inter-particles magnetic interactions. Similar behaviour is reported for several substituted Sr-hexaferrite systems [29, 30]. The considerable decline in the anisotropy field (H_a) for all sample is an outcome of the dependence of H_a on the saturation magnetization. A comparable behaviour with a more considerable relative drop is observed in the coercive field manner. Similar behaviour with a more significant relative decrease is observed in the coercivity behaviour. This can be clarified by the coercive field dependence on saturation magnetization. It can be seen from Figure 6 (e) and Table 2, the achieved values of H_a in this study is approximately large, confirming that all produced products are magnetically hard. The high values of magneto-crystalline anisotropy field (H_a) at x=0 showed the relatively drastic magnetic hardness which has a potential

application for a microwave absorber. Moreover, the variations of H_a values follow the same trend of H_c values. Another sensible reason for the reduction (or increase) of H_a is the decrease (or increase) of H_c [20]. The squareness ratio ($S=M_r/M_s$) (Table 2) of all the compounds ranged from 0.57-0.52. The compounds having (S) ≥ 0.5 are in a single magnetic domain and if the (S) ≤ 0.5, then the compounds are in multi magnetic domain [31]. The squareness ratio of the synthesized samples with x=0.0 to 0.75 is greater than 0.5, thus making them a single magnetic domain.

4. CONCLUSION

This work reports the influence of Co ions substitution on the structure, morphology and magnetic properties of strontium hexaferrite M-type prepared by sol-gel auto combustion method. XRD patterns of these samples showed a single Sr M-hexagonal at x=0, while with the increase of the cobalt contents, both of the desired phase of the strontium M-type and the undesired phase appeared. Irregular particles distribution with non-uniform manner shape showed by FE-SEM images, while the surface morphology does not show appreciable changes with cobalt ions substitution. Raman spectroscopy confirmed that the $SrFe_{12}O_{19}$ and its substitution by Co ions have magnetoplumbite crystalline structure. The intensities of all major peaks decreased and slightly shifted towards higher frequencies as the cobalt ions content increased. All magnetic parameters such as the saturation magnetization, remanence magnetization, coercive field, effective anisotropy constant, anisotropy field, and squareness ratio are found to decrease with increasing Co ions contents. Weakened super-exchange interactions among particles were observed owing to the replacement of Sr by Co ions in hexaferrite system.

REFERENCES

[1] Y. Yang, X. Liu, & D. Jin, "Influence of heat treatment temperatures on structural and magnetic properties of $Sr_{0.50}Ca_{0.20}La_{0.30}Fe_{11.15}Co_{0.25}O_{19}$ hexagonal ferrites," Journal of Magnetism and Magnetic Materials **364** (2014) 11-17.

[2] I. Auwal, S. Güner, H. Güngüneş, & A. Baykal, "$Sr_{1-x}La_xFe_{12}O_{19}$ (0.0≤ x≤ 0.5) hexaferrites: synthesis, characterizations, hyperfine interactions and magneto-optical properties," Ceramics International **42**, 11 (2016) 12995-13003.

[3] F. Kools, A. Morel, R. Grössinger, J. Le Breton, & P. Tenaud, "LaCo-substituted ferrite magnets, a new class of high-grade ceramic magnets; intrinsic and microstructural aspects," Journal of magnetism and magnetic materials **242** (2002) 1270-1276.

[4] V. A. Rane, S. S. Meena, S. P. Gokhale, S. Yusuf, G. J. Phatak, & S. K. Date, "Synthesis of low coercive $BaFe_{12}O_{19}$ hexaferrite for microwave applications in low-temperature cofired ceramic," Journal of electronic materials **42**, 4 (2013) 761-768.

[5] A. Awadallah, S. H. Mahmood, Y. Maswadeh, I. Bsoul, M. Awawdeh, Q. I. Mohaidat, & H. Juwhari, "Structural, magnetic, and Mössbauer spectroscopy of Cu substituted M-type hexaferrites," Materials Research Bulletin **74** (2016) 192-201.

[6] S. Katlakunta, S. S. Meena, S. Srinath, M. Bououdina, R. Sandhya, & K. Praveena, "Improved magnetic properties of Cr^{3+} doped $SrFe_{12}O_{19}$ synthesized via microwave hydrothermal route," Materials Research Bulletin **63** (2015) 58-66.

[7] I. Gul, W. Ahmed A. Maqsood, "Electrical and magnetic characterization of nanocrystalline Ni–Zn ferrite synthesis by co-precipitation route," Journal of Magnetism and Magnetic Materials **320**, 3-4 (2008) 270-275.

[8] M. Asif, M. Nadeem, M. Imran, S. Ahmad ,S. Musaddiq, W. Abbas, Z. A. Gilani, M. K. Sharif, M. F. Warsi, & M. A. Khan, "Structural, magnetic and dielectric properties of NiCo doped $BiFeO_3$ multiferroics synthesized via micro-emulsion route," Physica B: Condensed Matter **552** (2019) 11-18.

[9]   Z. Rouhani, J. Karimi-Sabet, M. Mehdipourghazi, A. Hadi, & A. Dastbaz, "Response surface optimization of hydrothermal synthesis of Bismuth ferrite nanoparticles under supercritical water conditions: Application for photocatalytic degradation of Tetracycline," Environmental Nanotechnology, Monitoring & Management **11** (2019) 100198.

[10]   H. Mehranfar, M. Mohammed, & A. Mohammad, "Structural and magnetic properties of mgfecro$_4$ ferrite nanoparticles," Journal of Non-Oxide Glasses **11**, 3 (2019) 33-40.

[11]   N. Rezlescu, C. Doroftei, E. Rezlescu, & P. Popa, "Fine-grained erbium-doped strontium hexaferrite," Physica status solidi (a) **203**, 15 (2006) 3844-3851.

[12]   H. M. Khan, M. Islam, Y. Xu, M. A. Iqbal, I. Ali, M. Ishaque, & M. A. Khan, "Structural, magnetic, and microwave properties of NdZn-substituted $Ca_{0.5}Ba_{0.5}Fe_{12}O_{19}$ hexaferrites," Journal of Sol-Gel Science and Technology. **75**, 2 (2015) 305-312.

[13]   Z. T. Khodair, A. M. Mohammad, & A. A. Khadom, "Investigations of structural and magnetic properties of $Cu_{1-x}V_xO$ nanostructures prepared by sol-gel method," Chemical Data Collections **25** (2020) 100315.

[14]   M. Almessiere, Y. Slimani, H. El Sayed, & A. Baykal, "Structural and magnetic properties of Ce-Y substituted strontium nanohexaferrites," Ceramics International **44**, 11 (2018) 12511-12519.

[15]   A. M. Mohammad, S. M. A. Ridha, & T. H. Mubarak, "Dielectric Properties of Cr-Substituted Cobalt Ferrite Nanoparticles Synthesis by Citrate-Gel Auto Combustion Method," International Journal of Applied Engineering Research **13**, 8 (2018) 6026-6035.

[16]   Z. Wu, R. Zhang, Z. Yu, L. Shan, L. Dong, & X. Zhang, "Study on preparation and magnetic properties of $Sr_{1-x}Gd_xFe_{12-x}Cu_xO_{19}$ (0.00≤ x≤ 0.20) strontium ferrite prepared by solid phase method," Ferroelectrics **523**, 1 (2018) 82-88.

[17]   M. Buzinaro, N. Ferreira, F. Cunha, & M. Macêdo, "Hopkinson effect, structural and magnetic properties of M-type Sm^{3+}-doped $SrFe_{12}O_{19}$ nanoparticles produced by a proteic sol-gel process," Ceramics International **42**, 5 (2016) 5865-5872.

[18]   S. Kumar, S. Supriya, & M. Kar, "Correlation between temperature dependent dielectric and DC resistivity of Cr substituted barium hexaferrite," Materials Research Express **4**, 12 (2017) 126302–126308.

[19]   E. Stoner, & E. Wohlfarth, "A mechanism of magnetic hysteresis in heterogeneous alloys," IEEE Transactions on Magnetics, **27**, 4 (1991) 3475-31.

[20]   M. Almessiere, Y. Slimani, & A. Baykal, "Structural and magnetic properties of Ce-doped strontium hexaferrite," Ceramics International **44**, 8 (2018) 9000-9008.

[21]   R. Topkaya, "Effect of Zn substitution on temperature dependent magnetic properties of $BaFe_{12}O_{19}$ hexaferrites," Journal of Alloys and Compounds **725** (2017) 1230-1237.

[22]   H. Fang, Z. Yang, C. Ong, Y. Li, & C. Wang, "Preparation and magnetic properties of (Zn–Sn) substituted barium hexaferrite nanoparticles for magnetic recording," Journal of magnetism and magnetic materials **187**, 1 (1998) 129-135.

[23]   I. Auwal, H. Güngüneş, S. Güner, S. E. Shirsath, M. Sertkol, & A. Baykal, "Structural, magneto-optical properties and cation distribution of $SrBi_xLa_xY_xFe_{12-3x}O_{19}$ (0.0≤ x≤ 0.33) hexaferrites," Materials Research Bulletin **80** (2016) 263-272.

[24]   A. Mohammad, S. Aliridha, & T. Mubarak, "Structural and magnetic properties of mg-co ferrite nanoparticles," Digest Journal of Nanomaterials & Biostructures (DJNB) **13**, 3 (2018) 615 - 623.

[25]   M. Almessiere, Y. Slimani, H. El Sayed, & A. Baykal, "Morphology and magnetic traits of strontium nanohexaferrites: effects of manganese/yttrium co-substitution," Journal of Rare Earths **37**, 7 (2019) 732-740.

[26]   D. Winataputra, T. Ujiyanti, & W. Adi, "The structure, magnetic and absorption properties of Zn-Ti substituted barium-strontium hexaferrite prepared by mechanochemical process," IOP Conference Series: Materials Science and Engineering **202**, 1 (2017) 012090.

[27]   M. Yousefi, S. Afghahi, M. Amini, & M. B. Torbati, "An investigation of structural and magnetic properties of Ce-Nd doped strontium hexaferrite nanoparticles as a microwave absorbent ",Materials Chemistry and Physics **235** (2019) 121722-121738.

[28] A. Alsmadi, I. Bsoul, S. Mahmood, G. Alnawashi, K. Prokeš, K. Siemensmeyer, B. Klemke, & H. Nakotte, "Magnetic study of M-type doped barium hexaferrite nanocrystalline particles ",Journal of Applied Physics **114**, 24 (2013) 243910–243918.

[29] L. Peng, L. Li, X. Zhong, R. Wang, & X. Tu, "Crystal structure and physical properties of microwave sintered $Sr_{1-x}La_xFe_{12-x}Cu_xO_{19}$ (x= 0–0.5) ferrites for LTCC applications," Journal of Magnetism and Magnetic Materials **411** (2016) 62-67.

[30] L. Peng, & L. Li, "Magnetic, electrical and dielectric properties of microwave sintered $Sr_{1-x}La_xFe_{12-x}Ni_xO_{19}$ (x= 0− 0.35) hexaferrites used for nonreciprocal LTCF devices," Journal of Materials Science: Materials in Electronics **28**, 23 (2017) 17816-17826.

[31] M. N. Ashiq, R. B. Qureshi, M. A. Malana, & M. F. Ehsan, "Synthesis, structural, magnetic and dielectric properties of zirconium copper doped M-type calcium strontium hexaferrites," Journal of Alloys and Compounds **617** (2014) 437-443.